J Electroceram (2012) 28:226–232
DOI 10.1007/s10832-012-9716-5

Influence of the calcium excess in the structural and spectroscopic properties of the complex perovskite $Ba_3CaNb_2O_9$

Orlando Valdez-Ramírez · Francisco Gómez-García · Marco A. Camacho-López · Enrique Ruiz-Trejo

Received: 25 May 2011 / Accepted: 13 March 2012 / Published online: 13 April 2012

Abstract The effects of the change in the Ca/Nb ratio in the structure and spectroscopic properties of the solid solution $Ba_3Ca_{1+x}Nb_{2-x}O_{9-\delta}$ with x=0–0.25 are investigated. The solid solution undergoes a transition from an hexagonal phase (2:1 order) to a cubic phase (1:1 order) with increasing calcium content as indicated by X-Ray diffraction and Raman. The calcium excess matches with a gradual increase in blue colour due to a reduction at the high temperatures of sintering. Optical absorption experiments showed that there are different absorption bands in the region 0.45–4.5 eV corresponding tentatively to OH vibrations, polarons and monovalent oxygen vacancies. The series properties change gradually with calcium excess with the exception of $Ba_3Ca_{1.18}Nb_{1.82}O_{9-\delta}$ that showed a slight change attributable to the presence of protons in the lattice. These changes can be used to quantify protons in complex perovskites.

Keywords Point defects · Spectroscopy · Optical properties · Complex perovksites · Proton conductors

O. Valdez-Ramírez · F. Gómez-García · E. Ruiz-Trejo
Departamento de Física y Química Teórica, Facultad de Química,
Universidad Nacional Autónoma de México,
04510, México City, DF, Mexico

M. A. Camacho-López
Facultad de Química,
Universidad Autónoma del Estado de México,
Paseo Colón y Tollocan,
50120, Toluca, Estado de México, Mexico

Present Address:
E. Ruiz-Trejo (✉)
Department of Earth Science and Engineering,
Imperial College London,
SW7 2AZ, London, UK
e-mail: eruiztre@imperial.ac.uk

1 Introduction

Complex perovskites $AB_n'B_m''O_3$ are composed of at least two different B cations that can take a variety of valences [1]. The difference in the nature of the B cations leads to an ordering in the B site. Some of these complex oxides exhibit NaCl-type B-site ordering with cubic symmetry (space group *Fm-3 m)*, often referred to as 1:1-type, while others present a 2:1 ordering or hexagonal symmetry (space group P-3 m1).

The substitution of niobium for calcium in the solid solution $Ba_3Ca_{1+x}Nb_{2-x}O_{9-\delta}$ leads to the formation of oxygen vacancies; these in turn can dissociatively incorporate water into the lattice bringing about proton conduction [2]. In particular, $Ba_3Ca_{1+x}Nb_{2-x}O_{9-\delta}$ with x=0.18 (labeled BCN18) exhibits considerable levels of proton conduction even though hydrogen is not a constituent of the crystal lattice [3–6]. This and other complex perovskite families have a considerable potential as materials for fuel cells since the electrolytical properties can be finely tuned by modifying the Ca/Nb ratio to generate oxygen vacancies, by selecting the basicity of the contituent cations (Ba, Ca, Sr) to promote the incorporation of water and by controling the electronic conductivity of the family with a suitable choice of cations (Nb, Ta). However, the tuning of the properties in the series requires a systematic characterisation that can follow the smallest changes; in this sense, this work is an exploratory study aimed at following these changes in the structure by spectroscopic and diffraction methods. We characterised the solid solution structurally and spectroscopically to find a direct relation between properties and stoichiometry, in particular for a series known for its proton conducting properties.

The cubic and hexagonal structures of the complex perovskite $Ba_3CaNb_2O_9$ (labelled BCN) have been described

elsewhere [5]. It is however, not yet clear to what extent and in what conditions the members of the family display a cubic or an hexagonal symmetry. In either case, like most perovskites, $Ba_3CaNb_2O_9$ can be described as a network of corner sharing octahedra.

We will assume that the introduction of Ca for Nb leads to the formation of oxygen vacancies according to the following equation in the Kröger-Vink notation

$$3O_O^x + 2CaO + 2Nb_{Nb}^x \rightarrow 2Ca_{Nb}^{///} + 3V_O^{\bullet\bullet} + Nb_2O_5 \quad (1)$$

The oxygen vacancies facilitate oxygen transport and most importantly in this study, they can incorporate water according to [6],

$$H_2O + V_O^{\bullet\bullet} + O_O^x \leftrightarrow 2OH_O^{\bullet} \quad (2)$$

This makes the material a proton conductor [6]. There are other reactions that can take place, but among these, we will mention the loss of oxygen at high temperature described as,

$$O_O^x \leftrightarrow \frac{1}{2}O_2 + V_O^{\bullet\bullet} + 2e^- \quad (3)$$

These electrons can either move freely in the solid and produce electronic conductivity or be trapped in cations or oxygen vacancies. The oxygen vacancies can trap electrons to create monovalent oxygen vacancies according to

$$V_O^{\bullet\bullet} + e^- \leftrightarrow V_O^{\bullet} \quad (4)$$

In all cases, the electrons have an influence in the optical properties of the material.

In this article, we present first the structural properties of the series $Ba_3Ca_{1-x}Nb_{2+x}O_{9-\delta}$ with x ranging from 0 to 0.25 to determine the nature of the structure using XRD and then Raman as a complementary technique. We finally present the results of the optical properties to gain insight into the electronic defects of the series. Before the conclusions, we discuss our results in terms of the defects present in the system and the techniques used to study the series.

2 Materials and methods

Synthesis The starting compounds were $BaCO_3$ (99.98 %, Aldrich), $CaCO_3$ (Reagent Grade, Mallinckrodt) and Nb_2O_5 (99.9 %, Strem). A batch of samples with × from 0 to 0.25 was ground, pelletised uni-axially and then sintered at 1200 °C for 12 h, re-ground and finally sintered at 1450 °C for 24 h in air (atmospheric pressure=0.77 atm in Mexico City, 1.5 % water content). The heating and cooling temperatures were 5 °C/min. The samples prepared were of nominal composition $Ba_3Ca_{1+x}Nb_{2-x}O_{9-\delta}$ where x=0, 0.05, 0.10, 0.15, 0.18, 0.20, 0.25 and labelled BCN, BCN5, BCN15, etc. All samples were prepared simultaneously under the very same conditions. The density of the samples was determined by the Archimedes' method using de-ionised water as the immersion fluid.

Characterisation The structure was studied by XRD (D-5000 Siemens) with Cu-Kα radiation (λ=1.5406 Å) filtered with a Ni monochromator. The range 10–60 deg in 2theta, a step of 0.02 deg and a time per step of 0.6 s were used.

Raman Analysis MicroRaman spectroscopy was used as a second structural test for the ceramic pellets. A micro-Raman system (LabRaman HR-800 of Jobin-Yvon-Horiba) with a He-Ne laser (λ=632.8 nm) as the excitation source and an Olympus BX-41 optical microscope was utilised to collect the Raman spectra of the samples.

Spectrophotometry The colour of the pellets was analysed by spectrophotometry. The spectra were recorded in reflection mode with a spectrophotometer Varian Cary 5E UV–vis-NIR, in the interval from 0.62 to 4.96 eV. Before the analysis, the surface of the pellets was polished with sand paper to reveal a more homogenous colour.

3 Results

3.1 XRD

The majority of the reflections overlap for the cubic and hexagonal phases. For this reason, Fig. 1 shows only an amplified X ray diffraction pattern for the whole series highlighting the weakest reflections. There does not seem to be evidence of degradation in the form of calcium or barium hydroxides or carbonates and only a few unidentified reflections have been observed in the pattern. A simple inspection reveals that the BCN sample shows mostly an hexagonal structure and as the calcium content increases the hexagonal reflections decrease and the cubic structure appears gradually in the series. In particular, note that (hexagonal) reflections around 17.5, 24 and 33 deg decrease while the (cubic) reflection at 57 deg grows with increasing x. The trend seems to indicate a transition between the hexagonal and the cubic symmetries although we cannot quantify their concentration ratio with our current XRD data.

The pseudo-cubic lattice parameter as a function of calcium content is displayed in Fig. 2. Two series from the literature are included in the plot showing good agreement [7, 8]. Other values for BCN18 have been included as well [9–12]; the scatter in the literature is due to higher lattice parameters in protonated samples.

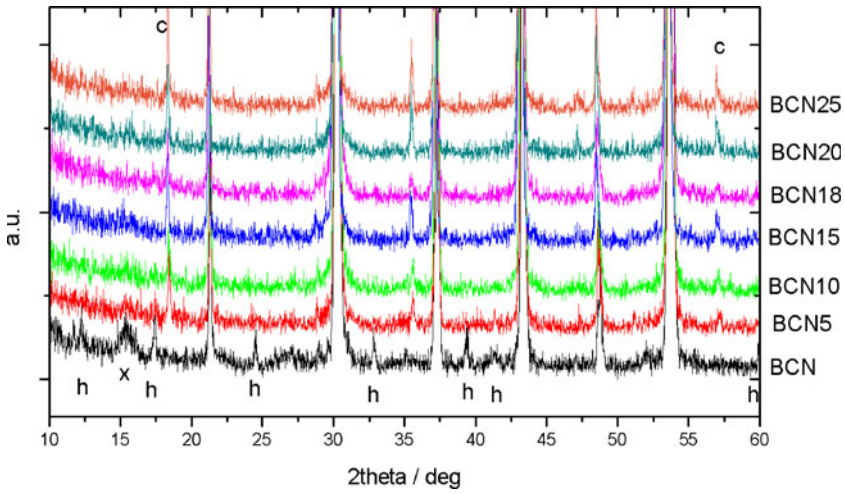

Fig. 1 XRD in the series $Ba_3Ca_{1+x}Nb_{2-x}O_{9-\delta}$ with x=0–0.25. The peaks associated mainly to the hexagonal symmetry are indicated below with a letter "h" while at the top the peaks unique to the cubic lattice are shown with a letter "c". The cross indicates a secondary phase and the rest of the peaks are common to both the cubic and the hexagonal phases

The percentage of theoretical density achieved was BCN=92 %; BCN5=72 %; BCN10=73 %; BCN15=80 %; BCN18=93 %; BCN20=80 % and BCN25=85 %.

3.2 Raman analysis

The assignation of the peaks in the Raman spectra to a specific mode is not a straightforward task. However, valuable information can be obtained by observing the variations in the different signals and compared to available data in the literature.

Figure 3 shows the Raman spectrum of all the series between 100 and 1000 cm^{-1}. For BCN the spectrum is clear with a flat background and well-defined peaks. There are two strong peaks at 825 cm^{-1} and 360 cm^{-1} and then 4 weaker signals at 130, 240, 280 and 407 cm^{-1}. For the rest of the series the major signal at 825 cm^{-1} splits into two peaks. Other signals decrease considerably (for example, 360 cm^{-1}) while some new signals appear at 700 cm^{-1} and 770 cm^{-1} with increasing x.

Two tentative plots are shown in Fig. 4 to indicate the relationship between Raman intensity and the stoichiometry. The peak at 700 cm^{-1} seems to have a direct relation with the oxygen vacancies; this peak is absent in the work of Levin, where no extrinsic oxygen vacancies exist [13]. BCN18 has a peak intensity slightly below the trend of the series indicating some oxygen vacancies are filled with OH species. The ratio of signals 825 and 750 cm^{-1} on the other hand experiences a change that has a closer relation with the decrease of hexagonal phase.

A study of the polymorphs of $Ca_3CaNb_2O_9$ by XRD and Raman shows a very clear difference in the Raman spectra between the 1:1 ordering and the 2:1 ordering [13]. This very same difference is seen in Fig. 3: for BCN there is only one peak at 825 cm^{-1} as in a 2:1 ordering while for the rest of the series, two independent (ca. 750 cm^{-1} and 825 cm^{-1}) signals develop for x >0 as in a 1:1 ordering [13]. A second feature indicating the gradual presence of a 1:1 ordering is that the signal at 750 cm^{-1} is bigger than the signal at

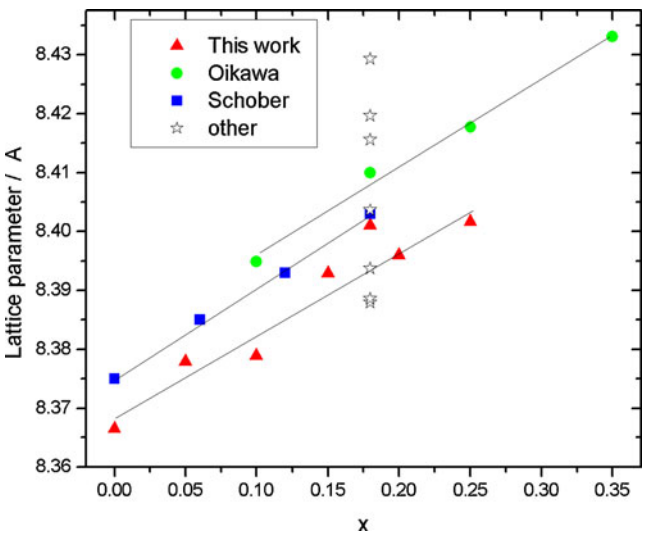

Fig. 2 Lattice parameter as a function of calcium excess

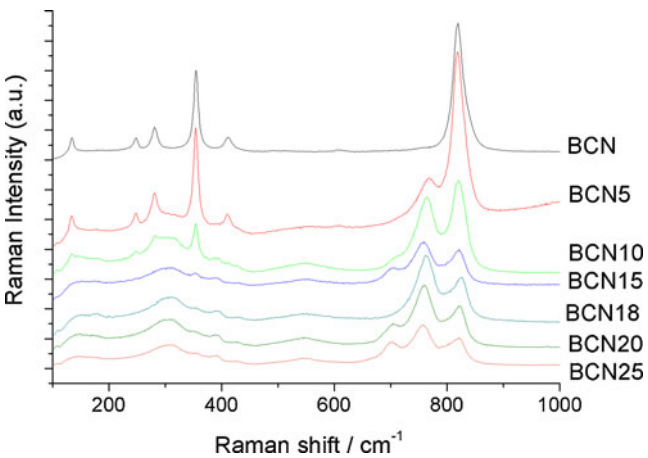

Fig. 3 Raman spectra of the series $Ba_3Ca_{1+x}Nb_{2-x}O_{9-\delta}$

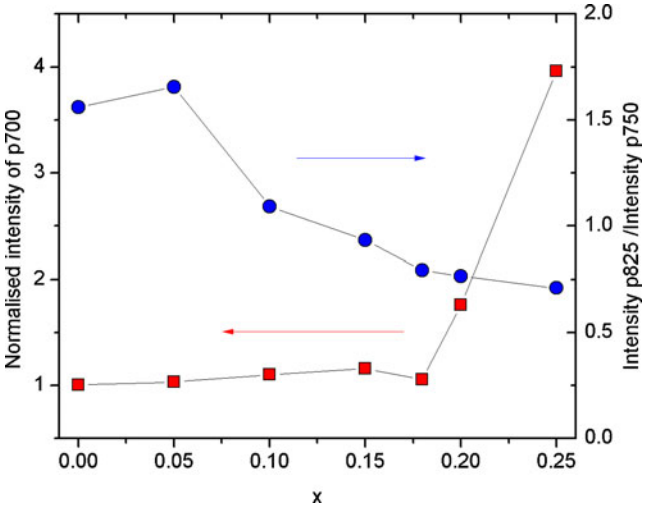

Fig. 4 Normalised intensity of the peak at 700 cm^{-1} (Left axis) and ratio between intensity of signal 825 and 750 cm^{-1} (right axis) as a function of calcium excess

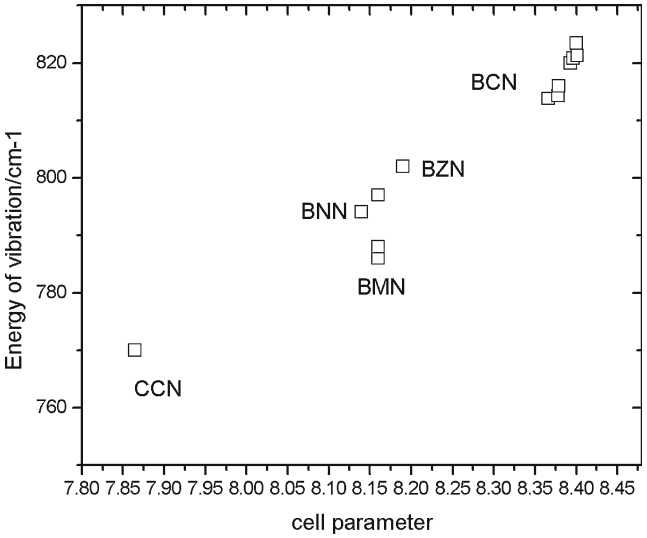

Fig. 5 Energy of breathing mode of octahedral cations as a function of the (pseudo)cubic lattice parameter for a variety of complex perovskites. BCN: all series in this work, BZN: $Ba_3ZnNb_2O_9$, BMN $Ba_3MgNb_2O_9$, BNN $Ba_3NiNb_2O_9$, CCN: $Ca_3CaNb_2O_9$. From ref [13–16]

825 cm^{-1} only when x >0.15 as in $Ca_3CaNb_2O_9$, with 1:1 ordering [13].

The peak at 825 cm^{-1} is assigned in the literature almost unanimously to the breathing mode of the octahedral of the B site cations in an hexagonal perovskite. Two peaks seem to develop around this value when the complex perovskites B cations order in a 1:1 network as if two breathing units were present. It is important to emphasize that various effects such as bond lengths or the very nature of the bond will change the vibration energies and hence the frequencies and wave numbers. CaO_6 octahedra are very different from NbO_6 both in terms of size (3.35 Å vs 2.8 Å [5]), bond nature and crystallographic position yet a clear consequence of the presence of CaO_6 and NbO_6 oscillators is not obvious. Nonetheless, a very clear trend between the energy of vibration and the (pseudo-cubic) lattice parameter can be observed for the series studied here and more complex perovskites as shown in Fig. 5 with data from references [13–16].

3.3 Optical absorption

The change in colour is clear and gradual in the series. The samples with the highest calcium content are more easily reduced (Eq. 3). BCN showed only a slight yellowish colour but the gradual increase in Ca was followed by a consistent increase in a blue/purple colour. Samples prepared previously in our laboratory at 1200 °C presented the same diffraction pattern as that of Fig. 1, but they did not show any change in colour. That is, the mere presence of the perovskite phase or the oxygen vacancies produced by the calcium excess does not lead to a change in colour; it is the treatment at high temperature (1450 °C) that darkens the samples, most likely through a reduction of the lattice (Eq. 3). This type of change in the colour has been previously observed in BCN18 [8] but only described qualitatively while in this work we give a more quantitative approach including other members of the series. It is also worth mentioning that a blue colouration in $Sr_{0.61}Ba_{0.39}Nb_2O_6$ was observed upon reduction [17].

Several bands in the absorption spectra can be observed in the studied region but their assignment to well-defined defect states is difficult. Some guidelines will be mentioned in the discussion section.

Figure 6 presents the absorption spectrum of BCN as well as a fit of the peaks found. This is a well-oxidised sample that shows a good reflectance over the infrared and visible regions. Two bands can be seen in the UV region, one broad band at 3.16 eV just on the edge of the UV and a second band at 3.99 eV. The slight creamy colour observed in BCN comes from the absorption tail in the UV region. In the visible/IR region two bands at 2.39 eV and a small one at 1.37 eV are found.

The optical absorption spectra of all the series are displayed in Fig. 7. As calcium content increases more bands appear in the absorption spectra and in addition to the signals at 2.39 eV and 1.37 eV seen in BCN, another, clear signal around 1.7 eV appears. All the samples follow a gradual increase except BCN18.

4 Discussion

4.1 Structure

Our XRD studies show clearly the formation of the perovskite phase with a gradual increase in the pseudo-cubic cell

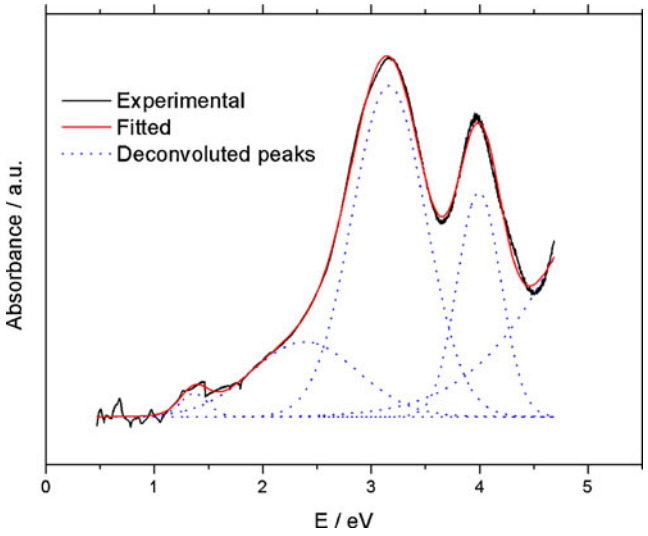

Fig. 6 The absorbance of BCN at room temperature

parameter. The data only gives us qualitative information about the presence of both phases and a transition from hexagonal to cubic in going from x=0 to x=0.25. This transition is expected since the addition of Ca at the expense of Nb interrupts the 2:1 order. As the Ca and Nb ions are very different in size, an ordering is still expected leading to the 1:1 phase.

The Raman spectra indicate more clearly the transition from the hexagonal to a cubic structure. The peak at 825 cm^{-1} associated to the hexagonal phase splits into two (750 and 825 cm^{-1}) associated with a cubic phase [13]; the intensity of the ratio of these two peaks may reveal the relative composition of the two phases. See Fig. 4.

For BCN18, the lattice parameter is very dependant upon the water content in the sample: in our work BCN18 increases just slightly off the rest of the series due to the water absorbed from the atmosphere as it is found in the literature. For the rest of the series, there does not seem to be a major water absorption and the corresponding swelling of the lattice.

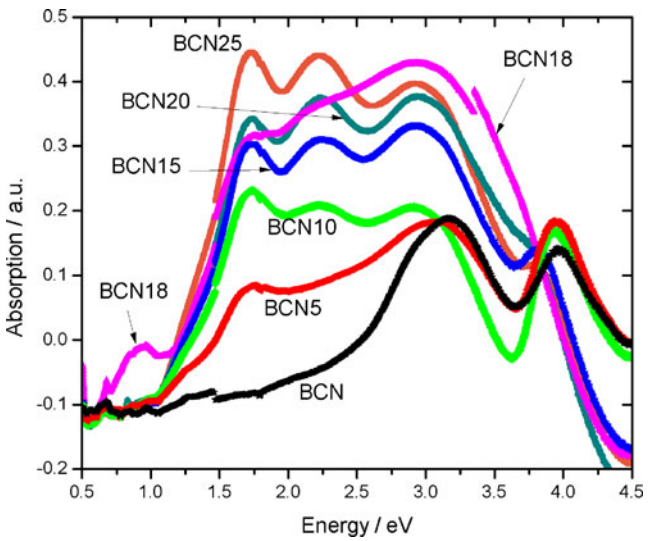

Fig. 7 The absorption spectra of all the series $Ba_3Ca_{1+x}Nb_{2-x}O_{9-\delta}$

4.2 Defects

4.2.1 Oxygen vacancies

Oxygen vacancies are the key defects in the series since they are involved in balancing the calcium excess, in the incorporation of water (Eq. 2) and in hosting the extra electronic defects. The presence of oxygen vacancies influences the local symmetry and this is seen in the Raman spectra in Fig. 3: samples with high levels of oxygen vacancies show broader bands as a result of reduced local symmetry. The presence of oxygen vacancies $V_O^{\bullet\bullet}$ in the series $Ba_3Ca_{1+x}Nb_{2-x}O_{9-\delta}$ (for $x \neq 0$) also suggests the possibility of the formation of monovalent oxygen vacancies and this will be discussed next.

4.2.2 Electronic defects

The high temperature sintering used reduces the material and the coloration is stronger in samples with the highest concentration of extrinsic oxygen vacancies. In terms of simple chemical equilibrium (Le-Chatelier's principle), this is counterintuitive as Eq. 3 indicates that the presence of extrinsic oxygen vacancies should make the sample less reducible. However, it is possible that the whole lattice achieves certain stability upon reduction by either generating microdomains, forming associates between the different charged defects, by creating stable colour centers or simply by promoting a more stable phase. A similar observation is reported for single crystals of Gd-doped Ceria: doped ceria was more reducible than the nominally pure ceria [18]. In $Ba_{0.5}Sr_{0.5}Co_{0.8}Fe_{0.2}O_{4-\delta}$ perovskites the larger lattice constant have a higher oxygen vacancy concentration as a consequence of the reduction of the transition metal oxides; as in our case, the larger lattice constant seems to favour the reduction of the transition metal [19].

A difficult problem is to develop a model that explains all the bands observed in the absorption spectrum (Fig. 7) since all of them involve electronic transitions of some sort –with the probable exception of the vibration of OH at 0.8 eV for BCN18. An additional and complicating factor, not taken into consideration in this work, is the roughness of the surface.

A universal criterion to identify small polaron absorption bands in oxide materials has been suggested [20]. According to this the ratio, W^2/M (W is the half-width at half-maximum height of the peak and M is the peak

energy in eV) plays a key role: a value of 0.14 eV is expected for a polaron. For BCN, the peak at 2.39 eV gives a value of 0.10 eV that might indeed represent a polaron formed by an electron trapped in a Nb site. The energy of a polaron is highly dependent upon the energy involved in the deformation of the surrounding lattice. This is of great relevance to the description of the BCN system, since there are two types of Nb sites in the cubic structure (space group *Fm-3 m)* with very different characteristics in terms of distance to next nearest neighbours and energy of substitution [5]. If the samples are completely or partially cubic, there must be two energies associated with each type of free polaron, one of them is at 2.39 eV as mentioned above. A second polaron can be adscribed to the signal at 1.37 eV. Even though the peak at 1.37 eV does not fit the 0.14 W^2/M criterion, the energy value is comparable to the polaron found in $LiNbO_3$ [21] or to the band at 1.69 eV ascribed to small polaron in reduced $MgNb_2O_6$ [22].

The other two major peaks around 3 eV and 4 eV in Fig. 7 are probably related to the fundamental band gap. In fact, as the cubic phase increases (larger x), the peak around 3 eV increases systematically in intensity and shifts to lower energies reflecting probably the effect of the Nb-O bond change.

For Yttria-stabilised zirconia, calculations of the electronic properties show that electrons can be trapped in oxygen vacancies and double occupied F centers [23]. Studies in highly reduced ceria also show that, in addition to Ce^{3+} polarons, it is possible to trap electrons in oxygen vacancies to form monovalent vacancies as in Eq. 4 [24]. We can tentatively assign the peak at 1.7 eV to monovalent oxygen vacancies.

4.2.3 Protons

The interest in the solid solutions $Ba_3Ca_{1+x}Nb_{2-x}O_{9-\delta}$ studied here is mainly due to the proton conducting levels achieved by BCN18. Incidentally, the sample with this stoichiometry showed the clearest deviations from the trends indicating the strongest influence of water incorporation in the properties of the material. Three main observations were made regarding protons.

The first observation is the slight increase in lattice parameter relative to the trend observed in Fig. 2. We attribute this to a higher level of protonation in BCN18 with respect to the rest of the series. The change in lattice parameter may also be related to other factors not yet fully addressed in the literature such as phase transitions or the effect of the sintering temperature and thermal history of the material. For example, structural studies on $Sr_3Ca_{1+x}Nb_{2-x}O_{9-\delta}$ revealed a change in the symmetry when the sample had incorporated water [25].

The second observation can be made in the Raman spectra. All along the series the peak at 700 cm^{-1} changes gradually from zero intensity in BCN to a clear defined signal in BCN25, the trend is interrupted only by BCN18 with the intensity as low as that of BCN with no oxygen vacancies. In BCN18, the vacancies of oxygen may be filled at least partially with OH. We suggest then, the intensity of the peak at 700 cm^{-1} as an indirect measure of the proton concentration. See Fig. 3.

The third observation of the water incorporation influence in BCN18 is seen in Fig. 7. In almost all oxides the OH stretch mode is found in the range 3200–3700 cm^{-1} (0.40–0.46 eV) [26] while the second harmonic is around 6745 cm^{-1} (0.84 eV). The signal around 0.85 eV for BCN18 in Fig. 7 can be assigned to the second harmonic of an OH vibration as in the case of $LiNbO_3$ [26–28]. This indicates that BCN18 is indeed the composition with the highest proton incorporation of the series.

4.3 Techniques

Finally we would like to make a few comments about the techniques used in this work. Our XRD gave very basic information regarding the structure and longer analysis times are required to perform a Rietveld analysis. Neutron diffraction or syncrotron studies will give better and more quantitative results regarding the ratio of the cubic and hexagonal phases. It is however a disadvantage that all these methods reveal the long range order of the lattice while the transition observed here may involve the gradual formation of microdomains.

Raman is very sensitive to the changes in the stoichiometry of the solid solution. One of the problems of this technique is the assignment of the bands to specific vibrations and furthermore, in the case of oxygen vacancies, the local structure is distorted making the spectra more complicated. It was however possible to see a very clear change in the spectra between the cubic and the hexagonal structures. It may, in future studies, be possible to quantify the amount of protons by following the intensity of the band at 700 cm^{-1} or to estimate the ratio of cubic and hexagonal phases by analysing the intensity ratio of signals 750/825 cm^{-1}. See Fig. 3.

As in the case of the Raman spectroscopy, the optical absorption has the problem of finding a proper model that can assign to each band the corresponding electronic process. Nonetheless, the presence of protons is clearly observed in the infrared region for BCN18 and this signal can be used to quantify the proton concentration. As for the electronic transitions, a model is necessary to interpret the absorption bands; this in turn would provide valuable information in the interpretation of the electronic conductivity in the series.

5 Conclusions

1. The structural properties of $Ba_3Ca_{1+x}Nb_{2-x}O_{9-\delta}$ change gradually and consistently with Ca excess. The cell undergoes a gradual transition from an hexagonal or 2:1 order in BCN to a cubic or 1:1 order in BCN25. The transition is seen in XRD but more clearly observed in the Raman spectra. Two signals at 825 and 750 cm^{-1} indicate the presence of the 1:1 ordering while their intensity ratio may reveal the ratio of hexagonal to cubic phases of the series.
2. The samples are more susceptible to reduction when there is Ca excess and this is observed in the increasing coloration. The absorption spectrum of BCN presents different bands that can be interpreted as follows: two peaks may be associated with Nb polarons: 1.37 eV and 2.39 eV. The peaks around 3.16 and 3.99 eV are probably related to the fundamental band gap. For the rest of the series, the peak at 1.7 eV might be associated with electrons trapped in oxygen vacancies to yield monovalent oxygen vacancies.
3. It is suggested that the effect of water incorporation in BCN18 is seen by IR absorption (band at 0.8 eV), by Raman (signal at 700 cm^{-1}) and by a slight increase in the lattice parameter with respect to the rest of the series. A full confirmation of the relation between these values and the proton concentration needs further studies as a function of partial pressure of water. Once unequivocally established, these tecniques can be used to estimate the concentration of protons in complex perovskites.

Acknowledgments We acknowledge financial support from FQ-UNAM via program PAIP-3190-22. OVR thanks Subprograma 127 from FQ-UNAM. We are grateful to Horacio López-Sandoval for help with the optical measurements.

References

1. P.K. Davies, H. Wu, A.Y. Borisevich, I.E. Molodetsky, L. Farber, Ann. Rev. Mater. Res. **38**, 369 (2008)
2. A.S. Nowick, Y. Du, K.C. Liang, Solid State Ionics **125**(1–4), 303 (1999)
3. A.S. Nowick, Y. Du, Solid State Ionics **77**, 137 (1995)
4. H.G. Bohn, T. Schober, T. Mono, W. Schilling, Solid State Ionics **117**(3–4), 219 (1999)
5. E. Ruiz-Trejo, R.A. De Souza, J. Sol. State Chem. **178**(6), 1959 (2005)
6. E. Ruiz-Trejo, Y.M. Baikov, J.A. Kilner, J. Mater. Chem. **8**(2), 429 (1998)
7. K. Oikawa, T. Kamiyama, S. Ikeda, T. Shishido, S. Yamaguchi, Solid State Ionics **154**, 641 (2002)
8. T. Schober, J. Friedrich, Solid State Ionics **136**, 161 (2000)
9. K. Lind, I. Sosnowska, R. Hempelmann, W. Schafer, K. Knight, Phys. B. **234**, 937 (1997)
10. E. Zimmer, K. Scharf, T. Mono, J. Friedrich, T. Schober, Solid State Ionics **97**(1–4), 505 (1997)
11. T. Shimoyama, T. Tojo, H. Kawaji, T. Atake, N. Igawa, Y. Ishii, Solid State Ionics **179**(7–8), 231 (2008)
12. I. Sosnowska, W. Schafer, R. Przenioslo, K. Lind, R. Hempelmann, Phys. B. Condens. Matter **276**, 864 (2000)
13. I. Levin, J.Y. Chan, R.G. Geyer, J.E. Maslar, T.A. Vanderah, J. Sol. State Chem. **156**(1), 122 (2001)
14. A. Dias, F.M. Matinaga, R.L. Moreira, Chem. Mater. **19**, 2335 (2007)
15. M.Y. Chen, C.-T. Chia, I.-N. Lin, L.-J. Lin, C.-W. Ahn, S. Nahm, J. Eur. Ceram. Soc. **26**, 1965 (2006)
16. U. Treiber, S. Kemmler-Sack, J. Solid State Chem. **43**(1), 51 (1982)
17. M. Gao, S. Kapphan, R. Pankrath, J.L. Zhao, Phys. Stat. Solidi B. **217**(2), 999 (2000)
18. E. Ruiz-Trejo, J. Maier, J. Electrochem. Soc. **154**(6), B583 (2007)
19. S. McIntosh, J.F. Vente, W.G. Haije, D.H.A. Blank, H.J.M. Bouwmeester, Chem. Mater. **18**(8), 2187 (2006)
20. O. F. Schirmer, M. Imlau, C. Merschjann, and B. Schoke, J. Phys. Condens. Matter 21(12), (2009)
21. O.F. Schirmer, D. Vonderlinde, Appl. Phys. Lett. **33**(1), 35 (1978)
22. C. Zaldo, M.J. Martin, C. Coya, K. Polgar, A. Peter, J. Paitz, J. Phys. Condens Matter **7**(11), 2249 (1995)
23. G. Stapper, M. Bernasconi, N. Nicoloso, M. Parrinello, Phys. Rev. B. **59**(2), 797 (1999)
24. H. Tuller, A.S. Nowick, J. Electrochem. Soc. **126**(2), 209 (1979)
25. J.T.S. Irvine, D.J.D. Corcoran, J. Canales-Vazquez, Solid State Ionics **152**, 749 (2002)
26. M. Wohlecke, L. Kovacs, Crit. Rev. Solid State Mater Sci. **26**(1), 1 (2001)
27. V. Szalay, K. Lengye, L. Kovács, V. Timón, A. Hernández-Laguna, J. Phys. Chem. **135**, 124501 (2001)
28. A. Gröne, S. Kapplen, J. Phys. Chem. Solid. **56**(5), 687 (1995)